Iris Matching Based on Personalized Weight Map

Wenbo Dong, Zhenan Sun, *Member*, *IEEE*, and Tieniu Tan, *Fellow*, *IEEE*

Abstract—Iris recognition typically involves three steps, namely, iris image preprocessing, feature extraction, and feature matching. The first two steps of iris recognition have been well studied, but the last step is less addressed. Each human iris has its unique visual pattern and local image features also vary from region to region, which leads to significant differences in robustness and distinctiveness among the feature codes derived from different iris regions. However, most state-of-the-art iris recognition methods use a uniform matching strategy, where features extracted from different regions of the same person or the same region for different individuals are considered to be equally important. This paper proposes a personalized iris matching strategy using a class-specific weight map learned from the training images of the same iris class. The weight map can be updated online during the iris recognition procedure when the successfully recognized iris images are regarded as the new training data. The weight map reflects the robustness of an encoding algorithm on different iris regions by assigning an appropriate weight to each feature code for iris matching. Such a weight map trained by sufficient iris templates is convergent and robust against various noise. Extensive and comprehensive experiments demonstrate that the proposed personalized iris matching strategy achieves much better iris recognition performance than uniform strategies, especially for poor quality iris images.

Index Terms—Iris recognition, Hamming distance, personalized matching strategy, weight map, ordinal features, binominal mixture model.

1 Introduction

Iris recognition as a reliable personal identification method has more and more important applications in our society, such as border control, banking, law enforcement, welfare distribution, and so on. There are mainly two kinds of performance metrics for a practical iris recognition system. One is accuracy and the other is usability. Currently, state-of-the-art iris recognition algorithms can achieve nearly perfect accuracy in controlled scenarios [1], [2], [3], [4], [5], [6]. However, usability is still the largest bottleneck of iris recognition toward wide deployment. It is remarkable that some new-concept iris recognition systems such as iris at a distance [8], [9], [11], [10] and iris on the move [12] have been developed in recent years. But, the limited depth of field (DOF) of iris acquisition devices [7] determines that it is inevitable to capture many poor quality iris images for recognition. Therefore, improvement of the capability of iris recognition algorithms on poor quality iris images becomes the most realistic approach to increase the throughput of long-range iris recognition systems.

An iris recognition algorithm mainly includes three steps: preprocessing, feature extraction, and feature matching. The first two steps have been extensively investigated in the literature, but iris matching is comparatively less addressed. Because iris feature code is usually represented using binary strings, simple iris matching methods such as Hamming Distance [3] are commonly adopted. And, most iris matching methods treat iris feature codes derived from different image regions of various subjects as equally important and assign the same weight value to them. Such a uniform matching strategy definitely is not optimal in terms of iris recognition accuracy because it ignores significant differences of iris texture patterns among individuals and variations of image structures among iris regions of the same subject. For example, Fig. 1 shows some example iris images of different eyes, along with their normalized versions. The iris image of Fig. 1a has rich textures in the inner band but fewer stripes in the middle band; the iris image of Fig. 1b has more stripes in the lower part than the upper part; the iris image of Fig. 1c has more occlusions of eyelids and eyelashes than Figs. 1a and 1b. Since all of iris image regions are encoded with the same algorithm, differences of texture patterns between these regions determine that each image region has its unique distinctiveness and robustness for iris recognition. Therefore, an adaptive iris matching strategy will hopefully achieve better recognition performance.

In this paper, we propose a class-specific iris matching strategy. The fundamental method for iris matching is still based on Hamming distance, but now it is a distance weighted by a personalized weight map. For example, $codeA$ is a registered iris code in the database and $codeB$ is a query iris code. Traditionally, the dissimilarity D between $codeA$ and $codeB$ is illustrated in (1) based on Hamming distance.

$$D = \|codeA \oplus codeB\|. \quad (1)$$

• *The authors are with the Center for Biometrics and Security Research (CBSR), National Laboratory of Pattern Recognition (NLPR), Institute of Automation, Chinese Academy of Sciences (CASIA), PO Box 2728, Beijing 100190, P.R. China.*
E-mail: wbdong@aoe.ac.cn, {znsun, tnt}@nlpr.ia.ac.cn.

Manuscript received 15 Jan. 2010; revised 30 June 2010; accepted 22 Oct. 2010; published online 13 Dec. 2010.
Recommended for acceptance by S. Prabhakar.
For information on obtaining reprints of this article, please send e-mail to: tpami@computer.org, and reference IEEECS Log Number TPAMI-2010-01-0036.
Digital Object Identifier no. 10.1109/TPAMI.2010.227.

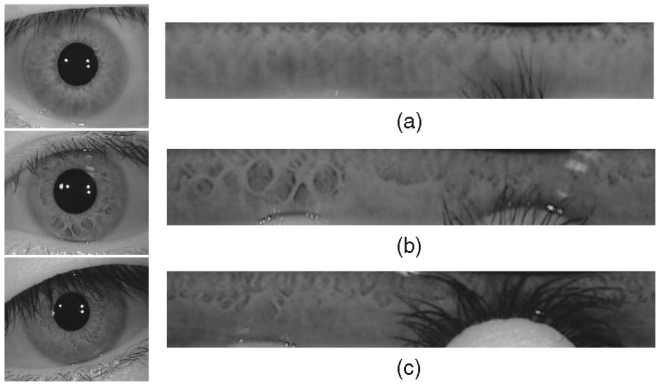

Fig. 1. Some example iris images and their normalized versions. They have different texture structures and different degrees of occlusion. (a) From CASIA3-Lamp 009-R-1. (b) From CASIA3-Lamp 005-L-4. (c) From CASIA3-Lamp 013-L-10.

If D is less than a threshold, the two iris images are considered to be from the same eye. Our improvement to the traditional Hamming distance is that a "weight map" W_A of the registered iris class A, which is denoted by an n-dimensional vector $\{w_1, w_2 \dots w_n\}^T$, is introduced to the matching function as follows:

$$D_A = \frac{\|(codeA \oplus codeB) \times W_A\|}{\|W_A\|}. \quad (2)$$

Since each registered iris class has its unique "weight map," the matching strategy based on (2) is named the "personalized matching strategy."

How to generate and represent the "weight map" is the key issue of this paper. Generally, a weight map is learned from a number of registered iris templates of the same class. Our experiments prove that such a weight map is robust and convergent as long as there are sufficient training data. Even if there are not enough registered iris images for training initially, the weight map can be updated online using recently recognized iris images as the new training data during system implementation.

Weight maps for adaptive iris matching may be represented using various forms and they all reflect the difference of stability between iris feature codes derived from different regions. But, different forms of weight maps lead to significantly different recognition performance. Another contribution of this paper is that a novel "binominal mixture model" is proposed to find the optimal weigh map based on the criteria of Discriminating Index (DI). Experiments prove the validity of our method.

The proposed personalized matching strategy is tested on some well-known iris image databases such as CASIA-IrisV3-LAMP, UBATH, and ICE2005. Experimental results show that our method has many desirable properties and clearly outperforms current iris matching strategies.

The paper is organized as follows: Section 2 presents related works on adaptive iris matching. Section 3 introduces how to generate and update the weight map. Section 4 investigates the approach to find the optimal weight map for iris matching. Section 5 discusses whether the weight map is stable and convergent. Section 6 presents extensive experiments and discusses how our method improves iris matching performance. Section 6 concludes this paper with some discussions.

2 Related Works

In this section, related works on iris matching are reviewed in order to put our proposed iris matching strategy in context.

2.1 Adaptive Region-Based Iris Matching Strategy

There are already some research works in the literature to adaptively incorporate weight maps into iris matching. However, various strategies are used to set the weight map of iris features.

2.1.1 Weight Map Based on Occlusion Mask

Daugman [3] proposed a "mask" to ignore bits occluded by eyelids and eyelashes, where occluded bits are masked by "0" and the visible bits are reserved by "1." If the masks of two iris feature templates are denoted as $maskA$ and $maskB$, then the weight map W in (2) can be represented as

$$W = maskA \cap maskB. \quad (3)$$

The weight map based on occlusions of eyelids and eyelashes is intuitive and straightforward. However, image segmentation is still an unsolved problem in computer vision and it is also a grand challenge to precisely segment the areas of eyelids and eyelashes from the original iris images. Although most state-of-the-art iris recognition algorithms have a module to remove the occlusions of eyelids and eyelashes [2], [13], [14], it does not always perform well for all iris images. The iris matching method based on occlusion mask has to face the risk of misleading segmentation results. In addition, complex algorithms for segmentation of eyelids and eyelashes need much additional computational cost.

2.1.2 Weight Map Based on Local Image Quality

Chen et al. [15] proposed that local iris image regions with better quality have better classification capability and vice versa. They incorporated the local quality measures (or local energy) as weights to compute the matching score. If the energy maps of the iris images A and B are denoted as $E_A = \{e_1^A, e_2^A, \dots, e_n^A\}$ and $E_B = \{e_1^B, e_2^B, \dots, e_n^B\}$, respectively, then the weight map W in (2) can be described as

$$w_i = \sqrt{e_i^A \times e_i^B}, \quad i = 1, 2, \dots n. \quad (4)$$

The basic idea of this quality-based mask representation method is good. However, the effectiveness of this method heavily depends on its defined quality measure. Much work has been reported on quantitative measurement of iris image quality [3], [5], [15], [16], [17]. However, the exact relationship between iris image quality and iris recognition performance still has not been strictly established. Furthermore, whether the region with higher local quality certainly has better classification performance is still a problem.

2.1.3 Weight Map Learned from All Iris Classes

Subjective estimation of the importance of various iris feature codes is not very accurate, so He et al. [18] proposed

a machine learning-based method to statistically select the most effective ordinal features of iris images and their weights to iris recognition performance. Such a study can explore which parts of iris regions and what kinds of ordinal filters commonly have better recognition performance for most iris image samples. It is demonstrated that such a learning-based weight map strategy can definitely improve the overall iris recognition accuracy. However, it should be noted that the feature selection method may generate a globally optimal result for training iris data set. So, the general weight map W_0 based on the machine learning approach does not fit a large number of individuals and cannot guarantee the optimal matching of two specific iris images:

$$W = W_0. \tag{5}$$

2.1.4 Weight Map Based on the "Best Bits"

Recent work by Hollingsworth et al. [19] demonstrated that there are some best bits in the iris code that are not easy to corrupt and are always consistent. They set consistent bits as 1 and inconsistent (fragile) bits as 0, and finally establish a mask-like template for every iris class.

Suppose there are n iris codes in the same class and the value of a certain bit i is 1 for m_1 times and 0 for m_0 times ($m_1 + m_0 = n$), so the stability of the bit is measured as

$$s_i = \frac{|m_1 - m_0|}{m_1 + m_0}. \tag{6}$$

The larger value of s_i denotes a higher stability in bit i and vice versa. If s_i is larger than a threshold (for example 0.3), they consider bit i a "consistent bit"; otherwise, they consider it a "fragile bit." So, their weight map W is actually described as

$$w_i = \begin{cases} 1, & s_i \geq 0.3, \\ 0, & s_i < 0.3. \end{cases} \tag{7}$$

The concept of consistent bits and fragile bits is a good reference for us, but how to choose the threshold is a problem. There does not exist a transient transition between good and bad bits, so it is not the best solution to binarize s_i into 1 and 0.

2.1.5 Weight Map Based on Information Fusion

Proenca and Alexandre [20] divided normalized iris images into six regions and combined the matching scores of all iris regions together to generate an overall matching score. Du et al. [21] studied the accuracy of iris recognition on different image regions and concluded that inner rings of irises are more distinguishable. These methods [20], [21] use information fusion strategy to coarsely set the weight map during iris matching.

In summary, there are already some works on adaptive region-based iris matching, but current models have drawbacks in generality of weight map or imprecise estimation of the weight map. It is the objective of this paper to find a class-specific weight map model.

2.2 Iris Image Preprocessing and Feature Representation Methods in Our Study

Many good works have been done on each module of an iris recognition algorithm and some of them are summarized in a recent survey on iris recognition [2]. Here, it is necessary for us to briefly introduce the iris recognition algorithm used in our study.

Iris image preprocessing includes iris localization, iris segmentation, and normalization. We use the Adaboost-cascade iris detector to determine the rough position of iris center, and then apply an elastic model named "pulling and pushing" to refine the edge of iris and pupil, and finally remove the eyelashes and shadows via a prediction model. Details of iris image preprocessing can be found in [18].

Sun and Tan [22] proposed a general framework of iris feature representation based on ordinal measures. They have demonstrated that ordinal measures are intrinsic features of iris pattern and robust against various noise. So, this paper studies the weight map of ordinal iris features, but the results are also applicable to other kinds of iris features. In our study, two types of well-proven ordinal features [22], i.e., 17-pixel length trilobe ordinal features and 8-pixel length bilobe ordinal features, are used as the iris feature representation and the length of each iris template is 512 bytes (256×16 bits).

3 Personalized Weight Map for Iris Matching

In this section, we introduce how to generate the personalized weight map. It is the first step of our personalized matching strategy.

3.1 Generating the Weight Map

Suppose there are k training iris images in an iris class, and their iris codes are denoted by $code_1, \ldots, code_k$. We make $k \times k$ times of intraclass matching using these k codes and obtain the average matching result by (8)[1]:

$$P = \frac{1}{k \times k} \sum_{a=1}^{k} \sum_{b=1}^{k} code_a \odot code_b, \quad P = \{p_1, \ldots, p_n\}, \tag{8}$$

where P is a vector with the same length as the iris codes. For the ith bit, p_i represents the probability of the matching result being 1. Every p_i is of different value and bigger p_i indicates that bit i is more stable.

Suppose there are k iris codes in the same class, and the value of a certain bit i is 1 for m_1 times and 0 for m_0 times ($m_1 + m_0 = k$), so the average result of bit i is $p_i = \frac{m_1^2 + m_0^2}{(m_1 + m_0)^2}$ by (8). It is obvious that p_i is always between 0.5 and 1. For convenience, we normalize it to $[0, 1]$ by

$$W = 2P - 1, \tag{9}$$

where W ($W = \{w_1, \ldots, w_n\}$) is called the "weight map."

This weight map W is related to the map S ($S = \{s_1, \ldots, s_n\}$) described in (6). The stability of the bit i is $s_i = \frac{|m_1 - m_0|}{m_1 + m_0}$ as in (6), while in our method, the weight map is

$$w_i = 2 \frac{m_1^2 + m_0^2}{(m_1 + m_0)^2} - 1.$$

1. $a \odot b$ means logical NOT of $a \oplus b$ in Boolean operations. For convenience, we use this expression so that the typical matching score $D \in [0, 0.5]$ is reversed to $1 - D$, which is consistent with the probability of being the same iris.

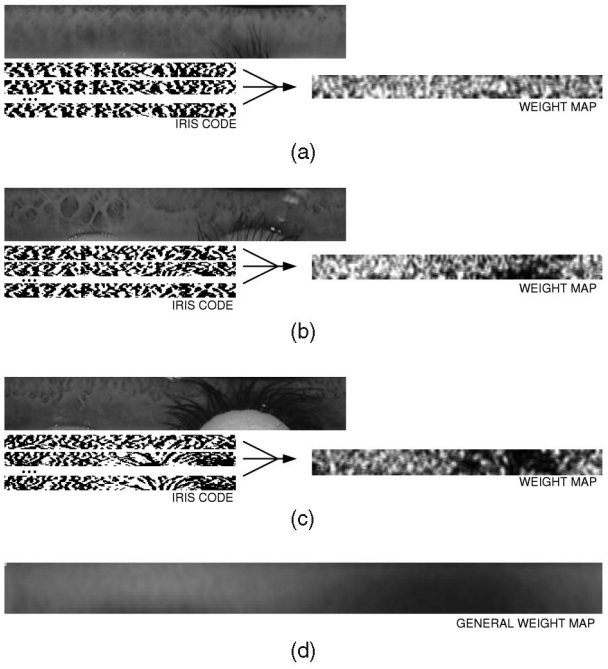

Fig. 2. Generate the personalized weight map. The weight maps (a), (b), and (c) are, respectively, learned from registered iris templates of their own classes. The general weight map (d) is calculated by averaging personalized weight maps of all iris classes.

It can be derived that $w_i = s_i^2$. It explains that w_i, p_i, and s_i are actually from the same source but with different forms. However, which is the best weight map among so many different forms and how to use the weight map is still a problem. We will discuss this issue in Section 4.

3.2 Properties of the Weight Map

Fig. 2 shows how to generate personalized weight maps. Three example weight maps are, respectively, generated from irises in Figs. 1a, 1b, and 1c. We can find some desirable properties of the weight map as follows:

- The bright area in the weight map indicates that the iris matching result is more stable in this region while the matching result in the dark area is less stable. The bright and dark areas are distributed unevenly, which explains that "fragile" bits indeed exist as described in [19].
- Areas likely to be occluded by eyelids or eyelashes are much darker than others, so they are less stable. This conclusion is consistent with our intuition. It also explains that the training of weight map may have deterministic function of removing occlusions of eyelids and eyelashes. Certainly, the weight map cannot replace the "eyelid mask," but it is still a choice to simplify the process of occlusion segmentation.
- It should be noticed that even in occluded areas, the value of weight map is not zero. It explains that some occluded regions also have recognition capability to some extent and they should not be completely neglected in iris matching.
- Although inner bands of iris images seem to have more complex textures than outer bands, there are no obvious difference between them in the weight map. If there is some difference, it may be caused by inaccurate iris edge detection.
- By averaging all "personalized weight maps," we can get a "general weight map," as shown in Fig. 2d. This weight map also shows the different classification capability of different regions, but it is statistically learned by all iris classes. The weight map mentioned in [18] could be regarded as one example of such general weight maps.

3.3 Updating the Weight Map

The generation of the weight map depends on a large number of registered images, which may not always be available. Fortunately, even if there are not enough registered images temporarily, users will leave many "successfully recognized" iris images in real applications, which can be used as training samples to update the weight map.

Since iris images in real-world applications are usually captured under various conditions, the updated weight maps are actually more representative. More training images result in more stable weight maps, and therefore frequent users of one iris recognition system will have much stable weight maps. In Section 4, we will discuss how many images are necessary for training the weight map.

Let W_n denote the weight map trained by n registered iris images, and $Code_{n+1}$ denote the new-coming iris code, so the new weight map W_{n+1} can be updated by

$$W_{n+1} = \frac{n^2 \times W_n + 2\sum_{m=1}^{n}(code_{n+1} \odot code_m - 1)}{(n+1)^2}. \quad (10)$$

Several important points should be noted here.

1. Iris codes may be of different rotation angles, and therefore they must be rotated to the same angle before further computation. We set one of the iris codes as the benchmark, and then match it with another iris code in several different angles using the common Hamming Distance. The angle with the max matching score is taken as the angle between the two iris codes. Finally, all iris codes are rotated to the same angle as the benchmark iris code. This work must be done in advance; otherwise, the weight map is not stable.
2. When the online learning procedure starts, there must exist a stop condition for weight map updating. For example, we can set $n = 20$ and only reserve the latest 20 templates and delete the older ones. There are also other methods which we do not enumerate here.
3. Although the process of updating weight map seems complex, it is only implemented offline after a successful recognition is performed and a new template is acquired. Therefore, the time of this process can be neglected in the practical systems.

3.4 Analysis of Computational Cost

Compared with the general Hamming distance, the weighted Hamming distance inevitably increases computational complexity of iris matching. Here, a detailed analysis is provided to demonstrate that the increase of computational cost is limited.

TABLE 1
Comparison of Computational Cost between the Traditional and Weighted Hamming Distance (HD)

Method	Memory storage (n templates per user)	Computational resource cost
Traditional HD	64× n byte	16XOR+16INC
Traditional HD with occlusion mask	128× n byte	16XOR+16INC +16AND+1DIV
Weighted HD with weight map	64× n+512byte	16XOR+256ADD +512AND+1DIV
Weighted HD with both weight map and mask	128× n+512byte	16XOR+256ADD +528AND+1DIV

The first issue is on memory storage. For general Hamming distance, one feature template is 64 bytes (512 bits) and its occlusion mask is the same 64 bytes. Suppose that there are n templates per user; one user occupies the memory of $128 \times n$ bytes. For weighted Hamming distance, one feature template is still 64 bytes, but the weight map is a vector of 512 fraction values which are quantified to integers of 0 to 255 (1 byte). So, the memory increases to $64 \times n + 512$ bytes. For a system with 1G RAM, it can load about 260,000 users (three templates for each user) with general Hamming distance, or 112,000 users with weighted Hamming distance. With fast development of computer technology, it is not a problem to provide enough memory for exhaustive searching.

The second issue is on matching speed. As we know, traditional iris matching is very fast for it only needs 512 XOR operations and 512 addition operations (ADD). Moreover, the 512 XOR operations can be processed in parallel by 32 bits once, and 512 ADD can be replaced by 512 incremental operations (INC) which are then carried out using the 16-bit lookup tables, so it only costs 16 XOR and 16 INC. It is undeniable that the classical iris matching is perfect for computation. As for weighted Hamming distance, it seems to require multiplication operations (MUL), but the MUL can be implemented by ADD, for the multiplicators are always 1 or 0. Here, we need 512 AND operations to determine whether it is 1 or 0 and need less than 512 (average 256) ADD operations to accumulate the weights with multiplicators being 1. At last, the result requires a division operation (DIV) ($\|W\|$ can be calculated when weight maps are loaded to the RAM), so the total computation is average $16\text{XOR} + 256\text{ADD} + 512\text{AND} + 1\text{DIV}$. Our new method is indeed slower than the traditional one, but it only costs less than 800 cycles once, which is still fast enough for practical use.

As a summary, the comparison of computational cost between general Hamming distance and weighted Hamming distance is listed in Table 1. From the table, we can see that the increase of computational cost is limited, which is worthy for improving system performance. The personalized iris matching strategy is clearly affordable in real applications.

4 Optimizing the Weight Map

4.1 The Optimization Problem among Various Forms of Weight Maps

The weight map reflects the stability of encoding algorithms on different regions of different iris classes. However, there are various forms of weight maps. For example, we can use the method in [19] to binarize the weight map: The bit larger than a threshold is set 1; otherwise, it is set 0, so the modified weight map will be $w'_i = \text{sgn}(w_i - t), \text{t} \in (0, 1)$. Another example is to use the power function of each bit as $w'_i = w_i^q, q \in constant$, which sets larger weights on more robust bits. Moreover, there are also other forms which we do not enumerate here.

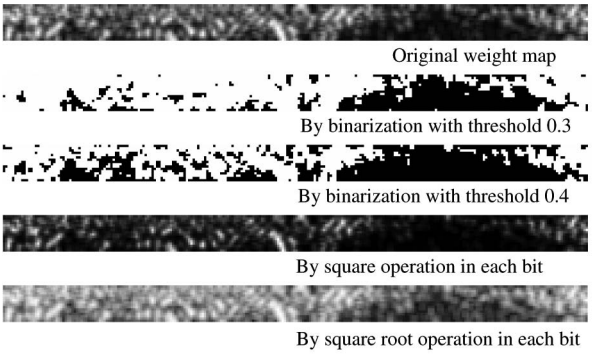

Fig. 3. Different forms of weight maps generated from the same original weight map.

Fig. 3 shows several different forms of weight maps. They are all specific cases of the original weight map. They all reflect the robustness of encoding algorithms on iris regions, but may yield different performance when they are used for iris matching.

How to choose the best form is an optimization problem, which can be defined as follows: Given the original weight map $W = \{w_1, w_2 \dots w_n\}$, find the optimal weight map $W' = \{w'_1, w'_2 \dots w'_n\}$ generated by W so that $F()$ indicating the performance of iris recognition achieves the maximum value:

$$\begin{cases} \max\limits_{w'_1,\dots,w'_n} : F(w'_1, \dots, w'_n), \\ G(w'_1, \dots, w'_n) = \sum\limits_{i=1}^{n} w'_i - 1 = 0, \\ w_i > 0, i = 1, \dots, n, \end{cases} \tag{11}$$

where $F()$ is the objective function and $G()$ is the condition function. Here, the key problem is how to choose the $F()$ and how to make use of the known condition.

There are many criteria for evaluating the performance of a biometrics system. A common criteria is the Discriminating Index d, which is defined as follows:

$$d = \frac{|\mu_{inter} - \mu_{intra}|}{\sqrt{(\sigma^2_{inter} + \sigma^2_{intra})/2}}, \tag{12}$$

where μ_{intra} and σ^2_{intra} denote the mean and variance of intraclass Hamming distance, and μ_{inter} and σ^2_{inter} denote the mean and variance of interclass Hamming distance. Larger d indicates better discriminability. For convenience, we just use $F() = d^2$ as the objective function.

4.2 Solving the Optimal Weight Map Based on "Binominal Mixture Model"

To resolve the above optimization problem, we introduce the "binominal mixture model" here. This model can also be found in the open literature, such as [23], [24], but it was first used in biometrics to the best of our knowledge. The

definition of this model and its statistical properties are given in Appendix A.

We assume that the distributions of interclass and intraclass matching results follow the binominal mixture distribution. Based on this model, the parameters μ and σ^2 of the interclass and intraclass distributions can be explicitly expressed by w_i and w'_i, which will facilitate the mathematical deduction.

If we use the Discriminating Index d as the criterion, then the objective function $F() = d^2$ can be rewritten as the expression of w_i and w'_i (see Appendix A):

$$F(W') = \frac{2\left(\sum_{i=1}^{n} w'_i w_i\right)^2}{\sum_{i=1}^{n} w'^2_i \left(2 - w_i^2\right)}, \tag{13}$$

where w_i is the known prior probability of each bit and w'_i is the weighted term what we seek.

This optimization problem can be resolved by the Lagrange Multiplier method (see Appendix B for details). The final result is that when

$$w'_1 : w'_2 : \cdots : w'_n = \frac{w_1}{2 - w_1^2} : \frac{w_2}{2 - w_2^2} : \cdots : \frac{w_n}{2 - w_n^2}, \tag{14}$$

$F()$ achieves the maximum value.

Besides, there are other criteria to evaluate the performance of a biometrics system. For example, another discriminative index (we name it DI2) is

$$d' = \frac{|\mu_{inter} - \mu_{intra}|}{\sqrt{\sigma^2_{inter}}}. \tag{15}$$

If we use DI2 as the criterion, then the objective function $F() = d'^2$ can be redefined as

$$F(W') = \frac{\left(\sum_{i=1}^{n} w'_i w_i\right)^2}{\sum_{i=1}^{n} w'^2_i}. \tag{16}$$

This optimization problem can be resolved with a similar method and the final result is that when

$$w'_1 : w'_2 : \cdots : w'_n = w_1 : w_2 : \cdots : w_n, i = 1, \ldots, n, \tag{17}$$

$F()$ achieves the maximum value.

As a conclusion, different criteria lead to different results. Based on DI or DI2, the optimal form of weight map W' should be obtained by $w'_i = \frac{w_i}{2 - w_i^2}$ or directly by $w'_i = w_i$. Further experimental results will demonstrate that they both achieve better recognition performance than other forms of weight map and DI2 may be much better.

5 Robustness of the Weight Map

The basis supporting our study is that the personalized weight map must be robust and stable. In this section, we will discuss the robustness of the weight map, including 1) whether and how the weight map is convergent when the number of training images increases and 2) whether the weight map is robust in cross-camera iris image databases.

5.1 The Robustness of the Weight Map and Its Requirement of the Number of Training Images

To study the robustness of weight map, a new iris image database named CASIA-Iris-MultiReg is constructed. In this database, there are more than 30 iris classes and every class has hundreds of iris images. Moreover, all images in this database were acquired during developing and testing an iris recognition system at a distance [11]. These iris images were continuously captured in a two-year term. Various intraclass variations were introduced to the CASIA-Iris-MultiReg in uncontrolled iris acquisition scenario, such as with eye glasses or contact lens, defocusing, motion-blur, overexposure, and heavy occlusions of eyelids and eyelashes. The iris images in CASIA-Iris-MultiReg are representative in practical iris recognition applications. In conclusion, CASIA-Iris-MultiReg is well-suited for the study of iris matching problem.

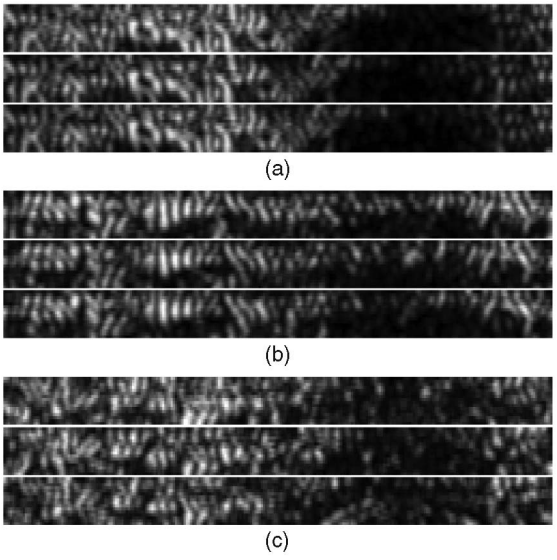

Fig. 4. Robustness of weight maps trained by different numbers of training images with specific encoding algorithm. (a) Three weight maps of iris class 1, respectively, trained by images 1-100, 101-200, and 201-300. (b) Three weight maps of iris class 2, respectively, trained by images 1-30, 31-60, and 61-90. (c) Three weight maps of iris class 3, respectively, trained by images 1-10, 11-20, and 21-30.

A simple experiment is first implemented based on subjective observation. For a certain iris class in CASIA-Iris-MultiReg, we trained three weight maps, respectively, by the images of 1-100, 101-200, and 201-300 (there are, in total, 366 training images in this iris class). The three weight maps are shown in Fig. 4a. We can see that these three weight maps are very similar. In contrast, Figs. 4b and 4c show weight maps of another two iris classes trained using 30 and 10 images, respectively. We can see that although the weight map in (c) are not as stable as (a) and (b) due to the small number of training images, they still appear similar. It indicates that the weight map is indeed stable from visual observations.

So the above experiment raises an important question of how many training images are required to train a stable weight map. To rigorously investigate the answer to this question, some objective experiments are implemented here in addition to the subjective visual observation.

For each iris class, we train its weight maps, respectively, by $5, 10, 15, \ldots, 80$ images and these weight maps are denoted as $\mathrm{w5}, \mathrm{w10}, \mathrm{w15}, \ldots, \mathrm{w80}$, respectively. Then, the intraclass comparisons are performed in all iris images of this database

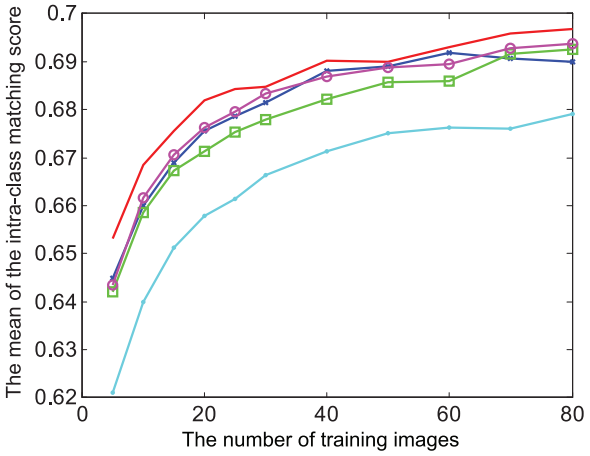

Fig. 5. Mean values of intraclass distribution become convergent with the increase of training images, which indicates that the weight map becomes stable as well.

and the mean values of matching score are respectively computed. Since there are many possible combinations of training set, i.e., $w5, w10, w15, \ldots, w80$ are not unique, we iterate the above experiments many times and get their average values. Mean values of the intraclass matching scores with the increasing number of training images are all plotted in Fig. 5. Only the statistics of five iris classes are investigated here for the convenience of illustration. In Fig. 5, we can see that intraclass mean values increase with the number of training images. It explains that a larger number of training images makes the weight map more stable and correspondingly achieves better iris recognition performance.

From the above discussions, we can conclude that the weight map is stable and robust as long as there are sufficient number of training images. As a rough estimation, we consider that 10 to 15 training images are necessary for generating a robust weight map.

5.2 The Robustness of the Weight Map in Cross-Camera Iris Image Databases

The personalized weight map is an intrinsic attribute of each iris class since the weight value is mainly determined by the correlation between the encoding filter and the structure of local image region. So, we assume that the weight map is robust against outer environmental factors such as the imaging sensor, etc. Here, an experiment is implemented to investigate the robustness of personalized weight map in cross-camera iris image databases, i.e., we want to find whether the weight map trained in one database captured by Sensor A can also be used in another database captured by Sensor B.

A cross-camera iris image database containing iris images of hundreds of persons is used for this experiment. The iris images in this database are acquired by five different iris cameras and each iris class has at least 10 images. Fig. 6 shows some example images acquired by two cameras produced by IrisGuard and OKI. The original iris images and its weight maps trained from 10 images are shown in this figure. We can see that the iris images acquired by different cameras have different quality of images, but their weight maps are very similar. It indicates that the personalized

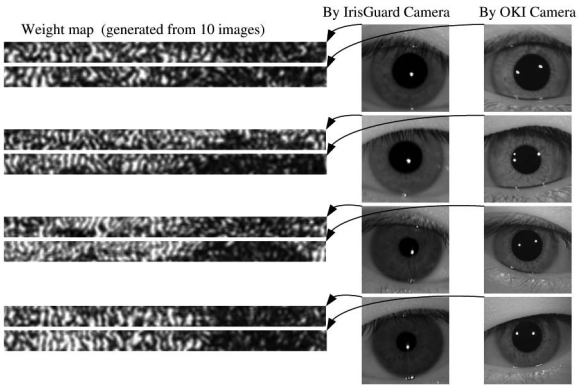

Fig. 6. The weight maps of the same iris are robust against different sensors.

weight map for each iris class are robust, though their training images are acquired by different sensors.

Some objective validation experiments are implemented to investigate the interoperability of personalized weight map. First, iris matching is performed in the IrisGuard database without and with weight maps, respectively, which are trained in IrisGuard database. Then, we iterate the experiment in IrisGuard database, but now the weight maps are trained in OKI database. The experiment results show that the two weight maps can both significantly improve iris matching performance, though the former may achieve better results. It indicates that the personalized weight map trained in one iris camera is also applicable to the applications based on another camera.

From a point of view, the personalized weight map is also one kind of iris feature representations. So, it does not change significantly according to the iris cameras if both the iris encoding method and local texture pattern are fixed.

However, we should notice that there are many kinds of iris feature codes generated by various types of filters (e.g., even symmetric or odd symmetric, dipole or tripole, and different wavelengths of the filter). It does not work if we use one filter for iris enrollment and another for iris recognition. In the same way, the iris weight map will also change if the types of filters are changed. When some bits of iris code are deemed "robust" for a dipole filter, they may not be "robust" for a tripole filter and vice versa. In a word, the personalized weight map depends on the iris feature and is "algorithm-specific."

As a conclusion, as long as the weight maps are generated by the same encoding filter, they are robust against environmental changes. That is to say that the personalized weight maps are interoperable in different imaging conditions. This result is encouraging for the study of cross-camera iris recognition.

6 Experimental Results

In this section, extensive experiments are conducted on a number of iris image databases to prove the validity of personalized weight map including:

1. how the personalized matching strategy can improve the matching performance;
2. whether the proposed method is the optimal weight map;

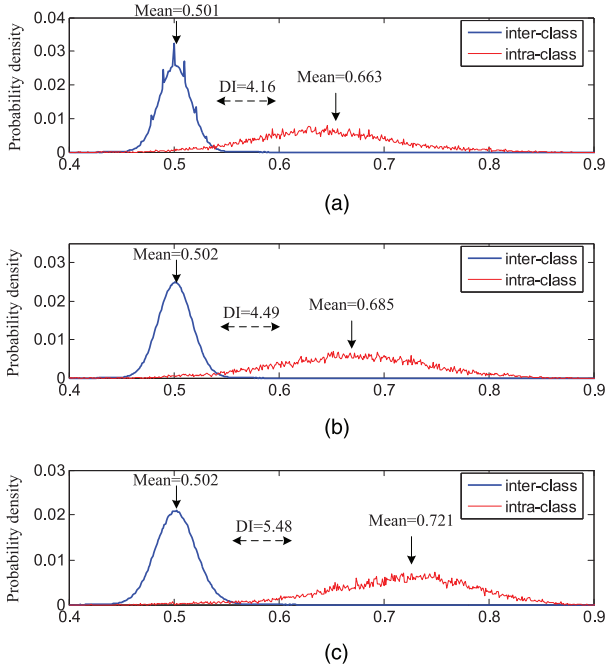

Fig. 7. The distribution of intraclass and interclass matching results on CASIA-IrisV3-Lamp iris database. (a) Hamming distance with no weights. (b) Hamming distance with general weights. (c) Hamming distance with personalized weights.

3. whether our method is more effective for low-quality images; and
4. whether our method is compatible with the method using multiple registered images.

6.1 The Validity of Personalized Matching Strategy

In this section, extensive experiments on large-scale iris image databases such as CASIA-IrisV3-Lamp [25], UBath [26], and ICE2005 [27] are performed to evaluate the validity of our method.

CASIA-IrisV3-Lamp [25] is released by the Institute of Automation, Chinese Academy of Sciences. It contains 16,213 iris images from 822 subjects and all subjects are Chinese people. In contrast to CASIA-IrisV1.0, it was collected in an indoor environment with illumination change, and contains many poor images with heavy occlusion, poor contrast, pupil deformation, and so on. It is a very challenging database, and there is no algorithm reported to yield very good performance on it, so it is very suitable for our experiment.

The UBath Database [26] is an iris database with good quality images. It includes about 32,000 iris images of 800 people, acquired with a machine vision camera under NIR illumination. The original image resolution is $1{,}280 \times 960$, so all images in this database are of very good quality. For reducing the computational cost, we only use downsampled images with resolution 640×480.

ICE 2005 Database [27] is also a challenging iris database like CASIA-V3.0-Lamp. It was used in the Iris Challenge Evaluation organized by NIST in 2005. The iris images of ICE2005 database were collected using a LG2200 sensor, including 1,528 images of 120 left eyes and 1,425 images of 124 right eyes. The data set was collected in weekly acquisition sessions and contains iris images of different

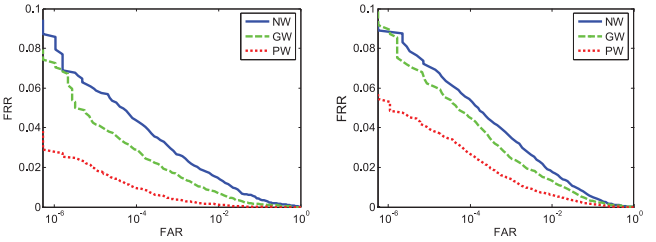

Fig. 8. ROC curves of iris matching on CASIA-IrisV3-Lamp iris database. (Left) In the trainng set. (Right) In the testing set.

quality. To be compliant with the ICE2005 protocol, the iris recognition algorithms are separately evaluated on the left and right eye subsets, respectively.

Experiments on various types of iris image databases ensure generality of the derived conclusions on a personalized weight map.

6.1.1 Experiments on the CASIA-IrisV3-Lamp

For every iris class, there are 19 or 20 images, from which we select 10 images as the training set to compute the weight map and the others as the testing set. Then, we make all possible interclass and intraclass comparisons. The distribution of intraclass and interclass matching scores in the testing data set is shown in Fig. 7.

For comparison, we also make iris matching experiments based on other methods. The first is the common strategy by Hamming distance without any weights (NW), the second is by Hamming distance based on the general weight (GW) map as described in Fig. 2d and the third is on the personalized weight (PW) map. Distributions of interclass and intraclass matching scores are plotted in Fig. 7. We can see that the proposed PW method can discriminate the intraclass and interclass comparisons more significantly than GW and NW.

Moreover, the recognition performance can be measured by the following two common indicators: 1) equal error rate (EER), that is, the crossover error rate when false accept rate is equal to the false reject rate; lower EER means higher accuracy; 2) discriminating index DI, defined in (12). Higher DI denotes higher discriminability of a biometric system. As a result, the EER of NW, GW, and PW is, respectively, 0.016, 0.014, 0.008, and the DI is, respectively, 4.16, 4.49, and 5.48. Obviously, PW is much better than GW and NW.

ROC curves of iris matching are shown in Fig. 8. The performance metric of horizontal coordinate is false accept rate (FAR) and the performance metric of vertical coordinate is false reject rate (FRR). ROC curves are commonly used for comparing different pattern recognition algorithms and lower curve indicates better performance. Both of the ROC curves in the testing set and the training set are drawn in Fig. 8. We can see that PW is much better than GW and NW, and moreover, there is no large difference between the training set and the testing set, which explains that personalized weight maps trained by a different data set are also applicable to other testing data set.

6.1.2 Results on UBath Database

In this database, every iris class has 20 images, from which we select 10 images as training set to compute the weight

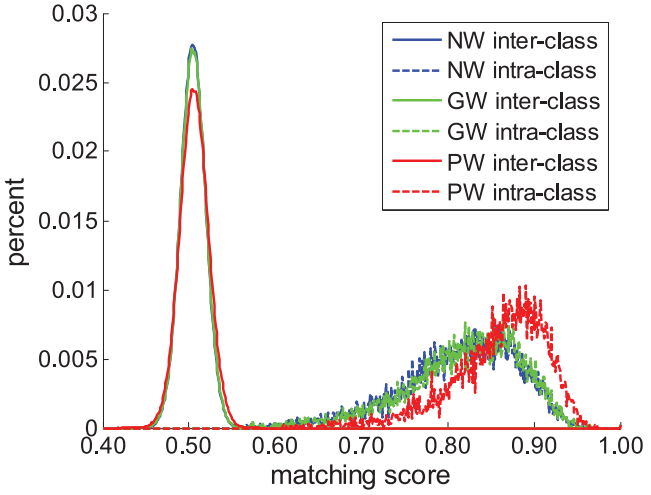

Fig. 9. The distribution of intraclass and interclass matching results on the UBATH database.

map and the other 10 images as the testing set. Then, we make all possible interclass and intraclass comparisons based on trained weight maps. In both the training set and the testing set, the number of intraclass comparisons is about 18,000 and the number of interclass comparisons is 16,000,000. (We only use 400 classes.)

For comparison, we still use the matching strategy with no weights, based on the general weight map and based on personalized weight map. The distribution of interclass and intraclass is drawn in Fig. 9. Moreover, ROC curves in both the training set and the testing set are plotted in Fig. 10. Since the image quality in UBATH is very good, all matching strategy can make quite good performance on this database, while our PW can even achieve 100 percent recognition rate in the training set.

The latest NIST report [30] also gives some experiment results on UBATH database, and the best one achieves $FRR \approx 0.002$ when $FAR = 10^{-4}$. Our algorithm can also achieve $FRR \approx 0.003$ when $FAR = 10^{-4}$. But, if it is cooperated with personalized weight map, then FRR will decrease to 0.001, which is better than the results in IREX report. It is a convincing evidence of superiority of the personalized matching strategy.

6.1.3 Results on ICE2005 Database

Similarly, we select 10 images from every iris class as the training set and train the weight map. Since many iris classes have less than 10 images, we only use personalized matching strategy on iris classes with more than 10 images.

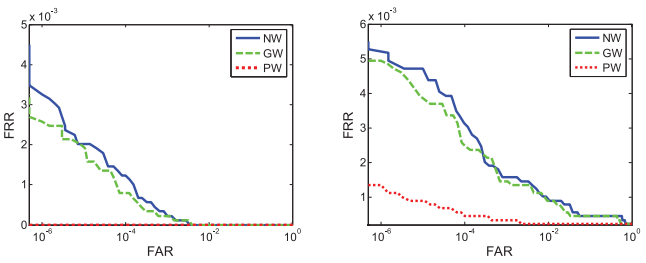

Fig. 10. ROC curves of iris matching on UBath database. (Left) In the training set. (Right) In the testing set.

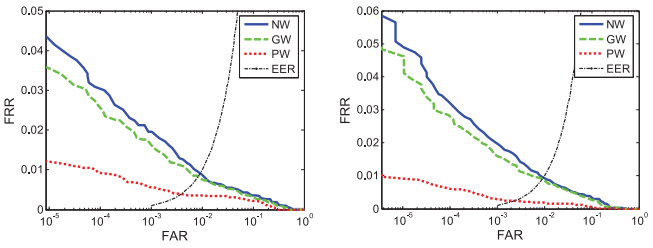

Fig. 11. ROC curves of iris matching on ICE2005-LEFT database. (Left) In the training set. (Right) In the testing set.

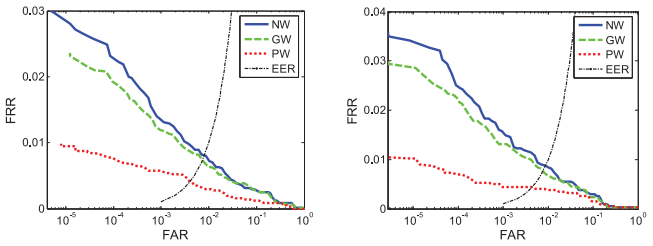

Fig. 12. ROC curves of iris matching on ICE2005-RIGHT database. (Left) in the training set. (Right) in the testing set.

Then, we make interclass and intraclass comparisons, respectively, in the training set and the remaining testing set.

The final results in ICE2005-Left are shown in Figs. 11a and 11b, and results in ICE2005-Right are shown in Figs. 12a and 12b. From the experiments, we can see that our algorithm achieves $FRR \approx 0.03$ when $FAR = 10^{-4}$, and if it is coordinated with the personalized weight map, then FRR will decrease to 0.01. It indicates that the proposed PW method also performs very well in the ICE database.

6.2 The Optimization of Personalized Weight Map

As mentioned in Section 4, the personalized weight map has many possible forms. We can directly use method (A), $w'_i = w_i$, or use the optimal method (B), $w'_i = \frac{w_i}{2-w_i^2}$, according to Section 4. And for comparison, we also use other forms of weight map, for example, (C) $w'_i = w_i^n, n \in constant$, and (D) $w'_i = \mathrm{sgn}(w_i - s), \mathrm{s} \in (0, 1)$. Method (D) is just the "best bits" method used in [19]. We implement experiments, respectively, by (A), (B), (C), and (D) with different parameters. The ROC curves on CASIA-IrisV3-Lamp are plotted in Fig. 13 and EER and DI (together with DI2) are presented in Table 2.

From Fig. 13 and Table 2, we can see that:

- Methods (A) and (B) have the best performance of ROC curves and make the lowest EER. It indicates that they may be the best forms of weight map, which is consistent with our mathematical analysis. It also indicates that our analysis based on the binominal mixture model and the optimal solution are valid and effective to deal with such problems.
- Methods (A) and (B) are, respectively, obtained based on the criteria of DI2

$$\left(d = \frac{|\mu_1 - \mu_2|}{\sqrt{\sigma_1^2}} \right)$$

and DI

$$\left(d = \frac{|\mu_1 - \mu_2|}{\sqrt{(\sigma_1^2 + \sigma_2^2)/2}} \right).$$

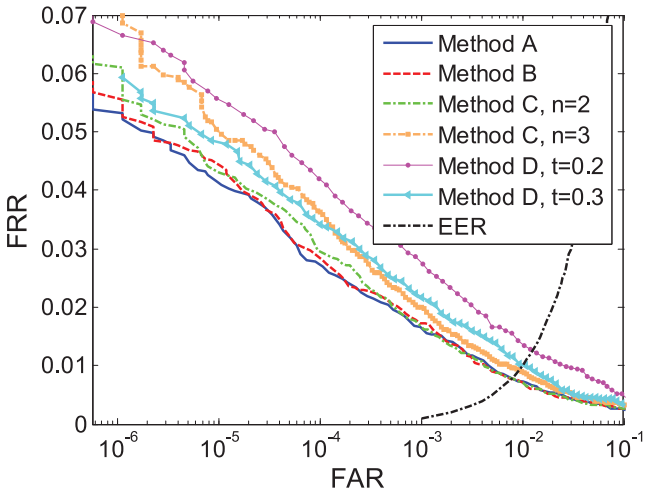

Fig. 13. ROC curves of iris matching based on different forms of personalized weight maps. Among them, Method (A) achieves the best performance.

From Table 2, we can see that the former achieves better performance in terms of ERR and ROC curve. The reason is that the interclass distribution may be more important than intraclass distribution for iris matching. So, DI2 may be a better criteria and method (A) is the best solution.

- Method (C) uses the square or cubed value of the weight map. It emphasizes the bits with larger value and sets larger weights on them, so it greatly increases the matching score of intraclass comparisons. But at the same time, it also overneglects the bits with less value and therefore sacrifices most randomness of interclass distribution. So although the discriminative index DI is large, the EER and ROC performance metrics are still worse than methods (A) and (B).
- Method (D), used in [19], does not achieve better performance than (A) and (B), no matter how we adjust the threshold, (for example, 0.2, 0.3, or other values). The reason is that there is no transient jump from "consistent bits 1" to "fragile bits 0." The "best bits" is just one specific example of weight map.
- Although the above weight maps are different, they are all personalized matching strategies which achieve much better performance than the method with no weight map or general weight map.

As a conclusion, the best method is method (A) ($w'_i = w_i$), which is the simplest expression, but achieves the best results. If not specifically mentioned, the PW in the following discussions indicates the weight map of form (A).

6.3 Performance on Low-Quality Databases

CASIA-Iris-MultiReg is a special database, which was introduced in Section 5. In this database, every iris class has hundreds of registered images and these images are of different quality. It is very suitable for the study of intraclass iris matching.

For every iris class, we select 20 images as training set and others as testing set. With training sets, we compute weight maps for each iris class. Then, all possible intraclass and interclass comparisons in the testing set are made to estimate the performance.

The distribution of intraclass and interclass matching scores is shown in Fig. 14 and the ROC curves are plotted in Fig. 15. We can see that PW achieves much better classification performance than GW and NW.

As an important observation, the performance improvement with PW is much more distinct in this database than in ICE, BATH, or the CASIA-IrisV3-Lamp database. The main reason is that there are more poor quality images in this database for which personalized matching strategy is advantageous over other methods. And this database is captured under less constrained conditions, so it represents iris image data in practical use. It is concluded that our PW strategy is useful for practical iris recognition systems, especially the iris recognition system at a distance [11] and on the move [12].

6.4 Comparisons with the Multiple Templates Matching and Fusion Method

Some researchers use multiple registered images for iris matching [28], [29] and output the fusion result of individual matching scores. For example, the final matching result is based on Sum-rule or Max-rule. As long as the query iris image is matched with one of the templates or the combined matching score exceeds a threshold, it is accepted as a genuine sample. Such a multiple templates matching and fusion method (MTMF) has been used in some practical systems and it really achieves much better performance than the system using only one registered image. So, the coming question is what is relationship between MTMF and the proposed personalized weight map and can the PW improve the performance of MTMF.

Although the proposed personalized weight map also uses multiple registered images, it is fundamentally different from MTMF. The multiple registered images are only used to

TABLE 2
Comparison of Recognition Performance Based on Different Forms of Weight Maps

Method	Inter-class mean	Intra-class mean	Inter-class variance	Intra-class variance	DI	DI2	EER
A	0.502	0.721	1.83×10^{-4}	3.02×10^{-3}	5.48	16.2	7.75×10^{-3}
B	0.502	0.738	2.22×10^{-4}	3.12×10^{-3}	5.76	15.8	7.78×10^{-3}
C(n=2)	0.502	0.767	3.05×10^{-4}	3.11×10^{-3}	6.39	15.1	7.84×10^{-3}
C(n=3)	0.503	0.802	4.79×10^{-4}	3.18×10^{-3}	6.99	13.7	9.22×10^{-3}
D(s=0.2)	0.501	0.666	1.20×10^{-4}	2.89×10^{-3}	4.23	14.8	12.6×10^{-3}
D(s=0.3)	0.502	0.674	1.28×10^{-4}	2.85×10^{-3}	4.48	15.3	10.1×10^{-3}
no weight map	0.501	0.663	1.19×10^{-4}	2.90×10^{-3}	4.16	14.7	16.2×10^{-3}

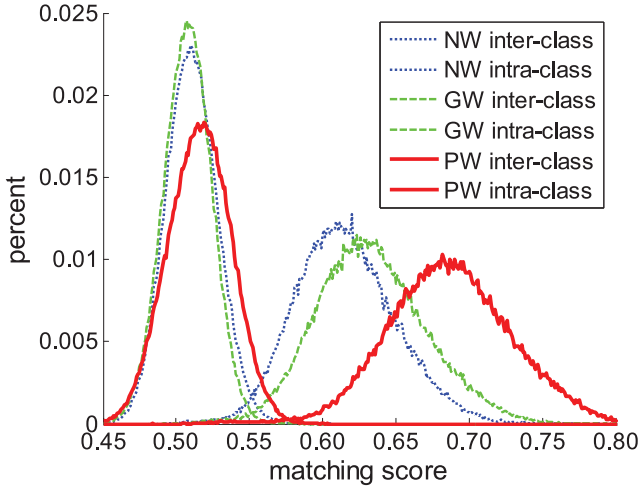

Fig. 14. The distribution of matching score on the CASIA-MultiReg database.

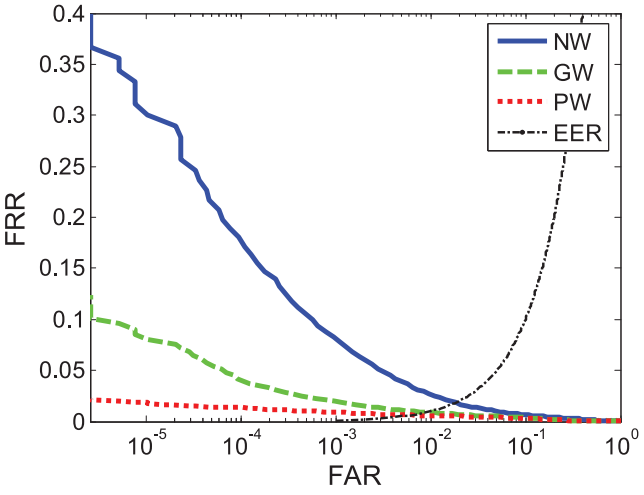

Fig. 15. ROC curves of iris matching performance on the CASIA-MulitReg database. PW is very effective in low-quality databases.

generate weight map, not directly used in iris matching. Actually, the weight map is also a kind of iris feature, which reflects the feature stability of the whole iris class.

We conduct iris matching experiments on CASIA-V3.0-Lamp, using one, three, and six registered images, respectively. Max-rule is used in MTMF approach. Both the NW and PW are applied to MTMF during iris matching and results are shown in Fig. 16. We can see that no matter whether there are one, three, or six templates, the system performance with PW is always better than NW. It indicates that the personalized weight map is complementary information to the MTMF method and it can significantly improve the performance of the MTMF approach.

6.5 Remarks

A number of informative conclusions can be drawn from the extensive experimental results presented above:

- Iris matching strategy based on personalized weight map greatly improves iris recognition performance. The fundamental reason is that the weight map is complementary feature information learned from multiple iris templates for each class. So, it is strongly recommended to incorporate the class-specific weight map into iris matching module of practical iris recognition systems.
- Personalized weight map becomes more and more stable with the increased number of training images. All available intraclass samples can be utilized to learn a stable weight map. And practical iris recognition systems can regard the newly recognized iris images as training data.
- Personalized weight map is an intrinsic feature for each iris class and robust against exterior factors. So personalized weight maps learned by one data set can also be used in an different data set, even if they are in the cross-camera iris recognition systems.
- The optimal form of personalized weight map is proven based on binominal mixture model and discriminating index criteria. The representation with the simplest expression achieves the best performance. Our analysis based on the binominal mixture model may also be helpful for the similar investigation of other biometrics.
- The advantages of personalized iris matching strategy are more significant for poor quality images. So this strategy may be well-suited to next-generation long-range iris recognition systems where most iris images are captured under uncontrolled environments and poor in quality.
- Personalized weight map is different in concept from the multiple templates matching and fusion methods. The weight map is not a redundancy, but can further improve the performance of MTMF approaches.

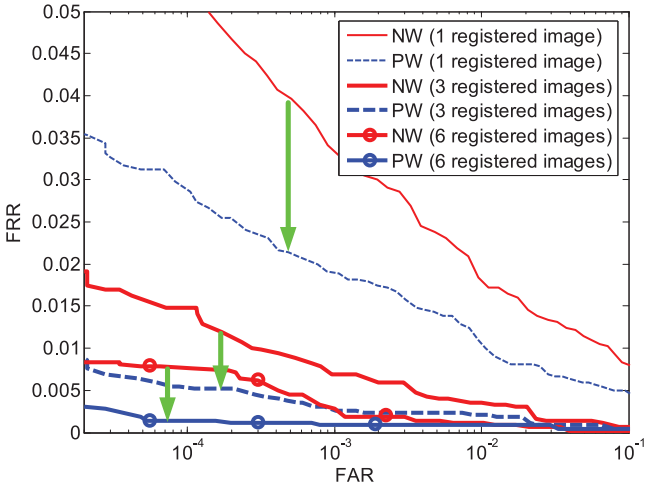

Fig. 16. ROC curves of iris matching performance on the CASIA-V3.0-Lamp database, respectively, using one, three, and six registered images.

7 Conclusions

In this paper, a novel personalized iris matching strategy based on weight map has been presented. The weight map of each iris class is learned based on intraclass iris matches among many registered templates. This weight map is updated and stabilized with the increase of the number of training images. Extensive and comprehensive experimental results have clearly demonstrated that our strategy is effective for iris matching and greatly improves the performance of iris recognition systems.

APPENDIX A
BINOMINAL MIXTURE MODEL

The Binominal mixture model is defined as

$$x = \sum_{i=1}^{n} \alpha_i x_i, \sum_{i=1}^{n} \alpha_i = 1, \tag{18}$$

where x_i $(i = 1, \ldots, n)$ obeys the Binominal distribution and α_i is the weighted term. The prior probability of x_i is p_i:

$$p(x_i) = \begin{cases} p_i, x_i = 1, \\ 1 - p_i, x_i = 0. \end{cases} \tag{19}$$

Supposing all x_i are independent,[2] the mean value μ and variance σ^2 of x can be calculated as (20). (This is the basic statistics principle.)

$$\begin{cases} \mu = \sum_{i=1}^{n} \alpha_i p_i, \\ \sigma^2 = \sum_{i=1}^{n} \alpha_i^2 \sigma_i^2, \end{cases} \quad \sigma_i^2 = p_i(1 - p_i). \tag{20}$$

We assume that if the distribution of interclass and intraclass iris matching scores obeys the binominal mixture distribution, then the Hamming distance D is equivalent to x, w_i' is equivalent to the weighted term α_i, and the prior probability p_i can be represented by the terms of original weight map w_i.

For the distribution of interclass comparisons, Daugman has proven that its randomness is like a binominal distribution with mean of approximately $\frac{1}{2}$ [1]. We let $p_i = p_0 = \frac{1}{2}$, and therefore the mean and variance of interclass distribution are

$$\begin{cases} \mu_{inter} = \sum_{i=1}^{n} w'_i p_0, \\ \sigma_{inter}^2 = \sum_{i=1}^{n} w'^2_i \sigma_0^2, \end{cases} \quad \sigma_0^2 = p_0(1 - p_0), \quad p_0 = \frac{1}{2}. \tag{21}$$

For intraclass comparisons, the prior probability p_i of each bit is different. So, its mean and variance are

$$\begin{cases} \mu_{intra} = \sum_{i=1}^{n} w'_i p_i, \\ \sigma_{intra}^2 = \sum_{i=1}^{n} w'^2_i \sigma_i^2, \end{cases} \quad \sigma_i^2 = p_i(1 - p_i), \tag{22}$$

where p_i can be represented as $p_i = \frac{w_i + 1}{2}$, just as the definition in (9).

Substitute (21) and (22) to (12), the objective function $F() = d^2$ can be explicitly expressed by w_i and w_i'.

$$F(W') = \frac{2\left(\sum_{i=1}^{n} w'_i w_i\right)^2}{\sum_{i=1}^{n} w'^2_i \left(2 - w_i^2\right)}, \tag{23}$$

where w_i is the known prior probability of each bit and w_i' is the weighted variable what we seek.

2. Actually, it is not strictly true. For example, Daugman has proven that the degree of freedom of interclass distribution is only approximately 249 [3]. Nevertheless, this model is still very effective in our study. In the future, we will continue to study such models when their elements are not independent.

APPENDIX B
SOLVE THE OPTIMIZATION PROBLEM

The optimization problem is defined as

$$\begin{cases} \max\limits_{\alpha_1, \ldots, \alpha_n} : F(\alpha_1, \ldots, \alpha_n) = d^2, \\ G(\alpha_1, \ldots, \alpha_n) = \sum_{i=1}^{n} \alpha_i - 1 = 0, \\ \alpha_i > 0, i = 1, \ldots, n, \end{cases} \tag{24}$$

where

$$F(\alpha_1, \ldots, \alpha_n) = d^2 = \frac{2\left(\sum_{i=1}^{n} \alpha_i w_i\right)^2}{\sum_{i=1}^{n} \alpha_i^2 (2 - w_i^2)}$$

is the objective function and $G()$ is the constrain condition.[3]

With the Lagrange Multiplier Rule, the maximum should be achieved when

$$\begin{cases} \frac{\partial(f - \lambda g)}{\partial \alpha_i} = 0, \quad i = 1, \ldots, n, \\ \frac{\partial(f - \lambda g)}{\partial \lambda} = 0. \end{cases} \tag{25}$$

Letting $A = \sum_{i=1}^{n} \alpha_i w_i$ and $B = \sum_{i=1}^{n} \alpha_i^2 (2 - w_i^2)$, the above equation can be resolved as

$$\frac{\partial(f - \lambda g)}{\partial \alpha_i} = \frac{2 w_i A \cdot B - A^2 \cdot 2\alpha_i \left(2 - w_i^2\right)}{B^2} - \lambda = 0. \tag{26}$$

Multiplying by α_i in both sides of the ith equation and then summing all n equations, we get

$$\lambda = \frac{2A \cdot A \cdot B - A^2 \cdot 2B}{B^2}. \tag{27}$$

Substituting λ to (26), we get

$$\alpha_i = \frac{B}{A} \frac{w_i}{2 - w_i^2}. \tag{28}$$

Therefore,

$$\alpha_1 : \alpha_2 : \cdots : \alpha_n = \frac{w_1}{2 - w_1^2} : \frac{w_2}{2 - w_2^2} : \cdots : \frac{w_n}{2 - w_n^2}. \tag{29}$$

In this time, $f(\alpha)$ obtains the maximal value

$$F_{\max}(\alpha) = \frac{2\left(\sum_{i=1}^{n} \alpha_i w_i\right)^2}{\sum_{i=1}^{n} \alpha_i^2 \left(2 - w_i^2\right)} = \frac{2\left(\sum_{i=1}^{n} \frac{w_i^2}{2 - w_i^2}\right)^2}{\sum_{i=1}^{n} \frac{w_i^2}{2 - w_i^2}} = 2 \sum_{i=1}^{n} \frac{w_i^2}{2 - w_i^2}. \tag{30}$$

If we define the discriminative index (DI2) as

$$d = \frac{|\mu_1 - \mu_2|}{\sqrt{\sigma_1^2}}, \tag{31}$$

then the objective function will be

$$F(\alpha_1, \ldots, \alpha_n) = d^2 = \frac{\sum_{i=1}^{n} \alpha_i w_i}{\sum_{i=1}^{n} \alpha_i^2}. \tag{32}$$

We also can resolve this optimization with a similar method and the final result is that when

3. Here, α_i is equivalent to w_i', which is the variable to solve.

$$\alpha_1 : \alpha_2 : \cdots : \alpha_n = w_1 : w_2 : \cdots : w_n, \tag{33}$$

the maximum value is obtained as

$$F_{\max}(\alpha) = \sum_{i=1}^{n} w_i^2. \tag{34}$$

ACKNOWLEDGMENTS

This work is funded by the National Natural Science Foundation of China (Grant Nos. 60736018, 61075024) and the International S&T Cooperation Program of China (Grant No. 2010DFB14110). The authors thank Zhaofeng He and Xiaobo Zhang for their help on this paper. The authors are also grateful to the reviewers for their valuable suggestions and comments. Zhenan Sun is the corresponding author for this paper.

REFERENCES

[1] J. Daugman, "Probing the Uniqueness and Randomness of IrisCodes: Results from 200 Billion Iris Pair Comparisons," *Proc. IEEE,* vol. 94, no. 11, pp. 1927-1935, Nov. 2006.
[2] K.W. Bowyer, K.P. Hollingsworth, and P.J. Flynn, "Image Understanding for Iris Biometrics: A Survey," *Computer Vision and Image Understanding,* vol. 110, no. 2, pp. 1-27, 2008.
[3] J. Daugman, "How Iris Recognition Works," *IEEE Trans. Circuits and Systems for Video Technology,* vol. 14, no. 1, pp. 21-30, Jan. 2004.
[4] R.P. Wildes, "Iris Recognition: An Emerging Biometric Technology," *Proc. IEEE,* vol. 85, no. 9, pp. 1348-1363, Sept. 1997.
[5] L. Ma, T. Tan, Y. Wang, and D. Zhang, "Personal Identification Based on Iris Texture Analysis," *IEEE Trans. Pattern Analysis and Machine Intelligence,* vol. 25, no. 12, pp. 1519-1533, Dec. 2004.
[6] D.M. Monro, S. Rakshit, and D. Zhang, "DCT-Based Iris Recognition," *IEEE Trans. Pattern Analysis and Machine Intelligence,* vol. 29, no. 4, pp. 586-595, Apr. 2007.
[7] W. Dong, Z. Sun, and T. Tan, "How to Make Iris Recognition Easier," *Proc. Int'l Conf. Pattern Recognition,* pp. 1-4, 2008.
[8] C. Fancourt, L. Bogoni, K. Hanna, Y. Guo, R. Wildes, N. Takahashi, and U. Jain, "Iris Recognition at a Distance," *Proc. Fifth Int'l Conf. Audio- and Video-Based Biometric Person Authentication,* pp. 1-13, 2005.
[9] S. Yoon, H.G. Jung, J.K. Suhr, and J. Kim, "Non-Intrusive Iris Image Capturing System Using Light Stripe Projection and Pan-Tilt-Zoom Camera," *Proc. IEEE Conf. Computer Vision and Pattern Recognition,* pp. 1-7, June 2007.
[10] AOptix Technologies, http://www.aoptix.com/, Aug. 2010.
[11] W. Dong, Z. Sun, and T. Tan, "A Design of Iris Recognition System at a Distance," *Proc. Chinese Conf. Pattern Recognition,* vol. 2, pp. 553-557, 2009.
[12] J.R. Matey, O. Naroditsky, K. Hanna, R. Kolczynski, D.J. LoIacono, S. Mangru, M. Tinker, T.M. Zappia, and W.Y. Zhao, "Iris on the Move: Acquisition of Images for Iris Recognition in Less Constrained Environments," *Proc. IEEE,* vol. 94, no. 11, pp. 1936-1947, Nov. 2006.
[13] Z. He, T. Tan, Z. Sun, and X. Qiu, "Towards Accurate and Fast Iris Segmentation for Iris Biometrics," *IEEE Trans. Pattern Analysis and Machine Intelligence,* vol. 31, no. 9, pp. 1670-1684, Sept. 2009.
[14] W. Kong and D. Zhang, "Detecting Eyelash and Reflection for Accurate Iris Segmentation," *Int'l J. Pattern Recognition and Artificial Intelligence,* vol. 17, no. 6, pp. 1025-1034, 2003.
[15] Y. Chen, S.C. Dass, and A.K. Jain, "Localized Iris Image Quality Using 2-D Wavelets," *Proc. IEEE Int'l Conf. Biometrics,* pp. 373-381, 2006.
[16] C. Belcher and Y. Du, "Feature Information Based Quality Measure for Iris Recognition," *Proc. IEEE Int'l Conf. Systems, Man, and Cybernetics,* 2007.
[17] N.D. Kalka, J. Zuo, N.A. Schmid, and B. Cukic, "Image Quality Assessment for Iris Biometric," *Proc. SPIE Biometric Technology for Human Identification III,* 2006.
[18] Z. He, Z. Sun, T. Tan, X. Qiu, and C. Zhong, "Boosting Ordinal Features for Accurate and Fast Iris Recognition," *Proc. IEEE Conf. Computer Vision and Pattern Recognition,* pp. 1-8, 2008.
[19] K.P. Hollingsworth, K.W. Bowyer, and P.J. Flynn, "The Best Bits in an Iris Code," *IEEE Trans. Pattern Analysis and Machine Intelligence,* vol. 31, no. 6, pp. 964-973, June 2009.
[20] H. Proenca and L.A. Alexandre, "Toward Noncooperative Iris Recognition: A Classification Approach Using Multiple Signatures," *IEEE Trans. Pattern Analysis and Machine Intelligence,* vol. 29, no. 4, pp. 607-612, Apr. 2009.
[21] Y. Du, B. Bonney, R. Lves, D. Etter, and R. Schultz, "Analysis of Partial Iris Recognition Using a 1-D Approach," *Proc. Int'l Conf. Acoustics, Speech, and Signal Processing,* vol. 2, pp. 961-964, 2005.
[22] Z. Sun and T. Tan, "Ordinal Measures for Iris Recognition," *IEEE Trans. Pattern Analysis and Machine Intelligence,* vol. 31, no. 12, pp. 2211-2266, Dec. 2009.
[23] A. Juan and E. Vidal, "On the Use of Bernoulli Mixture Models for Text Classification," *Pattern Recognition,* vol. 35, pp. 2705-2710, 2002.
[24] J. Hollmäen and J. Tikka, "Compact and Understandable Descriptions of Mixtures of Bernoulli Distributions," *Proc. Int'l Conf. Intelligent Data Analysis,* pp. 1-12, 2007.
[25] CASIA Iris Image Database, http://www.idealtest.org, 2010.
[26] Bath Iris Image Database, http://www.bath.ac.uk/elec-eng/research/igp/irisweb/database.htm, 2011.
[27] Nat'l Inst. of Standards and Technology, Iris Challenge Evaluation Data, http://iris.nist.gov/ice/, 2011.
[28] L. Ma, T. Tan, Y. Wang, and D. Zhang, "Efficient Iris Recognition by Characterizing Key Local Variation," *IEEE Trans. Image Processing,* vol. 13, no. 6, pp. 739-750, June 2004.
[29] N.A. Schmid, M.V. Ketkar, H. Singh, and B. Cukic, "Performance Analysis of Iris-Based Identification System at the Matching Score Level," *IEEE Trans. Information Forensics and Security,* vol. 1, no. 2, pp. 154-168, June 2006.
[30] P. Grother, E. Tabassi, G.W. Quinn, and W. Salamon, "Performance of Iris Recognition Algorithms on Standard Images," NIST Interagency Report 7629, pp. 1-120, Oct. 2009.

Wenbo Dong received the BE and MS degrees from Tsinghua University in 2003 and 2006, and the PhD degree from the Institute of Automation, Chinese Academy of Sciences (CASIA), in 2010, under the supervision of Professor Tieniu Tan. He is currently an assistant professor in the the Technology and Engineering Center for Space Utilization, Chinese Academy of Sciences (CAS). His research interests include computer vision, control system design, and embedded system development.

Zhenan Sun received the BE degree in industrial automation from Dalian University of Technology, the MS degree in system engineering from Huazhong University of Science and Technology, and the PhD degree in pattern recognition and intelligent systems from the Institute of Automation, Chinese Academy of Sciences (CASIA), in 1999, 2002, and 2006, respectively. He is an associate professor at CASIA. In March 2006, he joined the Center of Biometrics and Security Research (CBSR) at the National Laboratory of Pattern Recognition (NLPR) of CASIA as a faculty. He is a member of the IEEE and the IEEE Computer Society. His current research focuses on biometrics, pattern recognition, and computer vision.

Tieniu Tan received the BSc degree in electronic engineering from Xi'an Jiaotong University, China, in 1984, and the MSc and PhD degrees in electronic engineering from Imperial College of Science, Technology, and Medicine, London, United Kingdom, in 1986 and 1989, respectively. In October 1989, he joined the Computational Vision Group in the Department of Computer Science, The University of Reading, United Kingdom, where he worked as a research fellow, senior research fellow, and lecturer. In January 1998, he returned to China to join the National Laboratory of Pattern Recognition (NLPR), Institute of Automation of the Chinese Academy of Sciences (CASIA), Beijing, where he has been a professor and director of the NLPR since 1998, and is a former director general of the CAS Institute (2000-2007). He is also a deputy secretary-general (for cyber-infrastructure and international affairs) of the CAS. He has published more than 350 research papers in refereed journals and conferences in the areas of image processing, computer vision, and pattern recognition, and has authored or edited nine books. He holds more than 50 patents. His current research interests include biometrics, image and video understanding, and information hiding and information security. He is a fellow of the IEEE and the International Association of Pattern Recognition (IAPR). He has served as chair or a program committee member for many major national and international conferences. He is or has served as an associate editor or member of editorial boards of many leading international journals, including the *IEEE Transactions on Pattern Analysis and Machine Intelligence*, the *IEEE Transactions on Automation Science and Engineering*, the *IEEE Transactions on Information Forensics and Security*, the *IEEE Transactions on Circuits and Systems for Video Technology*, *Pattern Recognition*, *Pattern Recognition Letters*, *Image and Vision Computing*, etc. He is editor-in-chief of the *International Journal of Automation and Computing*. He was the founding chair of the IAPR Technical Committee on Biometrics, founding chair of the IAPR/IEEE International Conference on Biometrics (ICB) and the IEEE International Workshop on Visual Surveillance. He currently serves as the vice president of the IAPR, the executive vice president of the Chinese Society of Image and Graphics, deputy president of the Chinese Automation Association, and was deputy president of the China Computer Federation and the Chinese Automation Association. He has given invited talks at many universities and international conferences and has received numerous national and international awards and recognition.